



UNIVERSITY OF LEEDS

This is a repository copy of “Sounding” out crystal nuclei—A mathematical-physical and experimental investigation.

White Rose Research Online URL for this paper:

<https://eprints.whiterose.ac.uk/199190/>

Version: Accepted Version

---

**Article:**

Povey, MJ [orcid.org/0000-0002-9740-2596](https://orcid.org/0000-0002-9740-2596), Ettelaie, R [orcid.org/0000-0002-6970-4650](https://orcid.org/0000-0002-6970-4650), Lewtas, K et al. (3 more authors) (2023) “Sounding” out crystal nuclei—A mathematical-physical and experimental investigation. The Journal of Chemical Physics, 158 (17). ISSN 0021-9606

<https://doi.org/10.1063/5.0139811>

---

Published under an exclusive license by AIP Publishing. This article may be downloaded for personal use only. Any other use requires prior permission of the author and AIP Publishing. This article appeared in: Povey, MJ , Ettelaie, R , Lewtas, K et al. (3 more authors) (2023) “Sounding” out crystal nuclei—A mathematical-physical and experimental investigation. The Journal of Chemical Physics, 158 (17). and may be found at <https://doi.org/10.1063/5.0139811> . Uploaded in accordance with the publisher's self-archiving policy.

**Reuse**

Items deposited in White Rose Research Online are protected by copyright, with all rights reserved unless indicated otherwise. They may be downloaded and/or printed for private study, or other acts as permitted by national copyright laws. The publisher or other rights holders may allow further reproduction and re-use of the full text version. This is indicated by the licence information on the White Rose Research Online record for the item.

**Takedown**

If you consider content in White Rose Research Online to be in breach of UK law, please notify us by emailing [eprints@whiterose.ac.uk](mailto:eprints@whiterose.ac.uk) including the URL of the record and the reason for the withdrawal request.



[eprints@whiterose.ac.uk](mailto:eprints@whiterose.ac.uk)  
<https://eprints.whiterose.ac.uk/>

# 'Sounding' out crystal nuclei - a mathematical-physical and experimental investigation

Megan J Povey <sup>a</sup>, Rammile Ettelaie <sup>a</sup>, Ken Lewtas <sup>b</sup>, Andy Price <sup>b</sup>,  
Xiaojun Lai <sup>c</sup>, Fei Sheng <sup>c</sup>

a – School of Food Science and Nutrition, The University of Leeds, LEEDS LS2 9JT, UK. Corresponding author [m.j.w.povey@food.leeds.ac.uk](mailto:m.j.w.povey@food.leeds.ac.uk)

b – Lewtas Science & Technologies Ltd. 264 Banbury Road, Oxford OX2 7DY, United Kingdom

c – School of Chemical and Process Engineering, The University of Leeds, LEEDS LS2 9JT, UK

## Abstract

We outline techniques for the control and measurement of the nucleation of crystalline material. SAXS/WAXS XRD measurements are presented that demonstrate the impact of low power, continuous, non-cavitational ultrasound on the nucleation and crystallisation of a wax; n-eicosane dissolved in heptane/toluene solvent. A mathematical-physical approach based on rectification of heat and mass transport by such a low power oscillating pressure field is outlined and it is suggested that this approach be combined with dissipative particle dynamics (DPD) computational modelling to develop a predictive method capable of modelling the impact of low power oscillating pressure fields (acoustics and ultrasonics) on a wide range of nucleating systems. Combining ultrasound pitch and catch speed of sound measurements with low power harmonically oscillating pressure fields to monitor and control nucleation presents the prospect of entirely new industrially significant methods of process control in crystallisation. It also offers new insights into nucleation processes in general. However, for the acoustic control technique to be applied widely, further theoretical and modelling work will be necessary since at present, we are unable to predict the precise effect of low power ultrasound in any given situation.

## Introduction

Recently it has been shown that a low power, non-cavitating, continuous, oscillating pressure field will change the manner of crystal nucleation and growth through a process of rectified heat transfer. The application and method is patented in Povey and Lewtas (2022) <sup>1</sup>, the theory of rectified heat transfer is described in detail in Povey (2016)<sup>2</sup> and applications of the technique described in Povey (2017)<sup>3</sup>. Another approach is described in Haqshenas et al (2016)<sup>4,5</sup>.

The research questions that we answer in this work are (a) the effect of a harmonically varying low amplitude pressure field (not cavitating) on mass transfer to and from a crystal nucleus and (b) to investigate experimentally the practical effect of low power (sub-cavitational) pressure fluctuations on molecular and mesoscale ordering in both the unsaturated solution or pure melt and saturated solution/undercooled melt, thereby modifying crystal nucleation and growth. About (a) we present in the next section a theoretical development of an expression for the effect of harmonic pressure fluctuations on the mass transfer between a suspending phase and crystal embryo's/nuclei and draw tentative conclusions.

In Povey (2016)<sup>2</sup> the generalised view of Threlfall and Coles<sup>6</sup> was investigated using ultrasound measurements of the speed of sound in solutions of copper sulphate pentahydrate, in particular

events in the Dead Zone. In this work, we are interested in the regions A, B and C of Figure 2<sup>6</sup> because we hypothesise that low power, non-cavitating oscillating pressure fields are capable of altering the molecular packing in the melt/solution in addition to the dead zone, thereby providing a means of controlling nucleation and polymorph, for example by favouring 3L packing of triacylglycerols which is a precursor for the more stable  $\beta$  form of the fat rather than the 2L packing<sup>7</sup> which favours the less stable  $\beta'$  form.

A new analysis of the data of Figure 3 and Figure 4 in Povey<sup>2</sup> (Figure 1) indicates that critical fluctuations in the dead zone can be detected by pulse-echo ultrasound techniques with a pulse width of the order of 5  $\mu$ s. Each point plotted in Figure 1 is the result of a single measurement lasting around 5  $\mu$ s. The scatter in the data is far greater (by an order of magnitude as can be seen from the scatter in the data obtained in the region of uncontrolled crystal growth, regions D and E<sup>8</sup> in Threlfall and Coles for supersaturation > 0.15) than the measurement error and indicates that the coming into existence and subsequent disappearance of solid material associated with crystal embryos in the dead zone associated with relative supersaturation between 0.072 and 0.15 can be detected and measured.

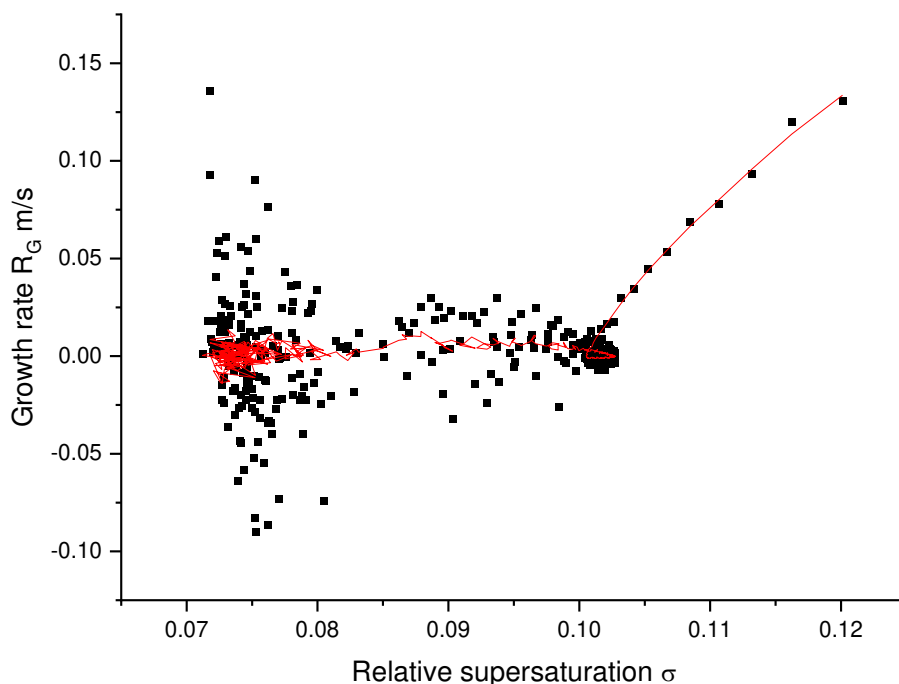


Figure 1 (Black filled squares) Crystal growth rate plotted against relative supersaturation (increasing supersaturation) for aqueous copper sulphate solution using 'instantaneous' i.e. not averaged over time measurements of pulse-echo time-of-flight<sup>9</sup>. (red line) instantaneous data smoothed using 15 point Savitzky-Golay routine.

Finally, we present Xray Diffraction Studies (XRD) of the crystallisation of a wax (eicosane) from solvent (heptane/toluene) in the presence and absence of an insonifying ultrasound field to investigate its effects both on the long-range order via small angle Xray scattering (SAXS) and simultaneously the effect on molecular packing with wide angle Xray scattering (WAXS). In comparison to the ultrasound data presented in Figure 1, it takes around 100 ms to take an entire frame of SAXS/WAXS data and consequently we don't expect to see critical fluctuations in structure

that are evidenced in the ultrasound data. However, we do see long time scale mesoscale effects due to insonification in the unsaturated solution which are absent in the quiescent fluid.

We conclude that the time scale of measurements is an important factor in characterising the structural dynamics of saturated solutions and suggest that changing, (in particular reducing) the measurement time window as is possible in pulse-echo ultrasound will provide quantitative information on the lifetime of crystal embryos, unlike even the most intense Xray sources such as the Diamond Light Source I22 beamline on which the experiments performed below were performed.

## Insonification and crystal nucleation

The treatment in Povey (2016)<sup>2</sup> of rectified thermal diffusion under the influence of an oscillating pressure field neglects mass transfer which we might also expect to be rectified.

Whilst CNT has come under multiple challenges<sup>7-18</sup> e.g. multiple step nucleation theory<sup>19,20</sup> the underlying physics as described by CNT is undeniable. Multiple step nucleation theories are microscopic, detailed theories addressing the attachment of individual molecules to surfaces, whilst CNT is a macroscopic theory, albeit applied to a relatively small object, e.g. a nucleus of  $\sim 4$  nm comprising a few hundred molecules. However, there is a great deal of evidence that CNT accurately describes crystal nucleation in the dispersed phase of emulsions<sup>21,22</sup>.

Here we provide a mathematical-physical description of mass transfer to and from an embryonic solid nucleus in the presence of a harmonically oscillating small pressure fluctuation and show that, despite the small pressure displacements involved, an impact on critical nucleus size can be expected. This treatment is consistent with the approach of Kashchiev in his book “Nucleation: Basic Theory with Applications” but differs in the respect that here the case of an harmonically oscillating small displacement pressure field is addressed.

First consider an infinitely large solid crystal in equilibrium with a solution whose solute concentration is  $c_0$ , at pressure  $P_0$ . Thus  $c_0$  defines the solubility of the solute molecules. At this concentration the Chemical Potential in the solution will be the same as the solid phase and is denoted  $\mu_0$ .

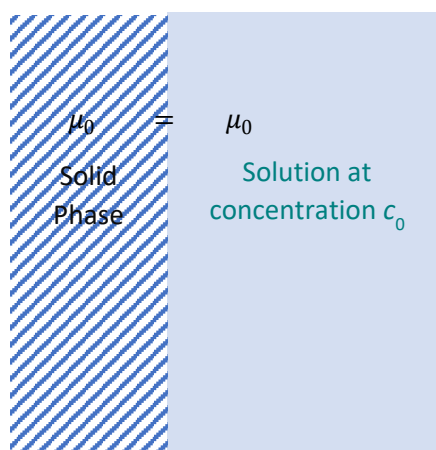


Figure 2 Chemical potential of solid and solution phases in equilibrium

What happens if the solid phase has a finite sized nucleus of radius  $r$ ? In that case the chemical potential in the solid phase becomes:

$$\mu_0 + \frac{2\gamma V_{solid}}{r}$$

Eq. 1

Where  $\gamma$  is the interfacial tension between the solid and the solution and  $V_{solid}$  is the molar volume of molecules in the solid phase. The solution that will be in equilibrium with this finite-sized nucleus will have a concentration that will ensure the same chemical potential as Eq. 1 in the solid. Denoting this as  $c_{solid}^0$ , where

$$\mu_0 + (RT) \ln \frac{c_{solid}^0}{c_0} = \mu_0 + \frac{2\gamma V_{solid}}{r}$$

and throughout  $(RT)$  is the product of the gas constant  $R$  and temperature  $T$ . Therefore:

$$\ln \frac{c_{solid}^0}{c_0} = \frac{2\gamma V_{solid}}{(RT)r}$$

Eq. 2

What happens if we also increase the pressure from its original value  $P_0$  to  $P = P_0 + \Delta P$ ? In this case the chemical potential in the solution  $\mu_{solution}$  will become:

$$\mu_{solution} = \mu_0 + (RT) \ln \frac{c_{solution}(P)}{c_0} + \int_{P_0}^P V_{solution} dP$$

Eq. 3

And in the solid phase:

$$\mu_{solid} = \mu_0 + \frac{2\gamma V_{solid}}{r} + \int_{P_0}^P V_{solid} dP$$

Eq. 4

The symbol  $V_{solution}$  in Eq. 3 represents the partial molar volume of the solute molecules in the aqueous solution. The concentration of solution adjacent to the nucleus and in equilibrium with it is obtained by equating Eq. 3 and Eq. 4, with the result:

$$\frac{2\gamma V_{solid}}{r} + \int_{P_0}^P V_{solid} dP = (RT) \ln \frac{c_{solution}(P)}{c_0} + \int_{P_0}^P V_{solution} dP$$

Eq. 5

Now expand  $V_{solid}$  and  $V_{solution}$  to the first order term in  $\Delta P$ :

$$V_{solid} = V_{solid}^0 + \frac{\partial V_{solid}}{\partial P} \Delta P + O(\Delta P^2)$$

Eq. 6

$$V_{solution} = V_{solution}^0 + \frac{\partial V_{solution}}{\partial P} \Delta P + O(\Delta P^2)$$

Eq. 7

If the crystal is pure, we note that  $\frac{\partial V_{solid}}{\partial P} = \frac{V_{solid}^0}{K}$  where  $K$  is the bulk modulus of the solid at  $P_0$ . Similarly, we define  $\beta = \frac{\partial V_{solution}}{\partial P}$  so that using Eq. 6 and Eq. 7, Eq. 5 becomes:

$$\frac{2\gamma V_{solid}^0}{r} + V_{solid}^0 \Delta P + \frac{1}{2} \frac{V_{solid}^0}{K} \Delta P^2 = (RT) \ln \frac{c_{solution}(P)}{c_0} + V_{solution}^0 \Delta P + \frac{1}{2} \beta \Delta P^2$$

Rearranging we get:

$$\ln \frac{c_{solution}(P)}{c_0} = \frac{2\gamma V_{solid}^0}{(RT)r} + (V_{solid}^0 - V_{solution}^0) \frac{\Delta P}{(RT)} + \frac{1}{2} \left( \frac{V_{solid}^0}{K} - \beta \right) \frac{\Delta P^2}{(RT)}$$

Eq. 8

So far, the concentration adjacent to the crystal, and in equilibrium with it, is set as  $c_{solution}(P)$ , while that in the bulk solution far away from the nucleus will be different, denoted as  $c_\infty$ .

Therefore, there will be a diffusion flux of molecules from solution towards the nucleus. or vice versa, if  $c_{solution}(P) \neq c_\infty$ .

Assuming a steady state flow, this mass flux is given by:

$$j = 4\pi r D \left( c_\infty - \overline{c_{solution}(P)} \right)$$

Eq. 9

where  $D$  is diffusion coefficient of solute molecules in the solution and  $\overline{c_{solution}(P)}$  is the average value of  $c_{solution}(P)$ . Rearranging Eq. 8:

$$c_{solution}(P) = c_0 \exp \left[ \frac{2\gamma V_{solid}^0}{(RT)r} + (V_{solid}^0 - V_{solution}^0) \frac{\Delta P}{(RT)} + \frac{1}{2} \left( \frac{V_{solid}^0}{K} - \beta \right) \frac{\Delta P^2}{(RT)} \right]$$

$$c_{solution}(P) = c_0 \exp \left[ \frac{2\gamma V_{solid}^0}{(RT)r} \right] \exp \left[ (V_{solid}^0 - V_{solution}^0) \frac{\Delta P}{(RT)} + \frac{1}{2} \left( \frac{V_{solid}^0}{K} - \beta \right) \frac{\Delta P^2}{(RT)} \right]$$

Eq. 10

In the case that the applied pressure fluctuation is small, i.e.

$$(V_{solid}^0 - V_{solution}^0) \frac{\Delta P}{(RT)} \ll 1$$

and

$$\left( \frac{V_{solid}^0}{K} - \beta \right) \frac{(\Delta P)^2}{(RT)} \ll 1$$

then the second exponential term in Eq. 10 can be expanded  $e^\theta \cong 1 + \theta + \frac{\theta^2}{2!} + \dots$ , yielding:

$$c_{solution}(P) \cong c_0 \exp \left[ \frac{2\gamma V_{solid}^0}{(RT)r} \right] \left\{ 1 + (V_{solid}^0 - V_{solution}^0) \frac{\Delta P}{(RT)} + \frac{1}{2} \left( \frac{V_{solid}^0}{K} - \beta \right) \frac{\Delta P^2}{(RT)} + \frac{(V_{solid}^0 - V_{solution}^0)^2 \Delta P^2}{2(RT)^2} + O(\Delta P^3) \right\}$$

Eq. 11

where we have only retained all terms up to  $O(\Delta P^2)$ . We can now determine the average flux from Eq. 9 by integrating over a single sinusoidal cycle period  $\mathcal{T}$  of a harmonically oscillating pressure field applied to the solution. With  $\Delta P = \Delta P_{max} \sin \omega t$  and using Eq. 11 .

$$\begin{aligned} \bar{j} &= \frac{1}{\mathcal{T}} \int_0^{\mathcal{T}} j dt = 4\pi r D \left[ c_{\infty} - c_0 \exp\left(\frac{2\gamma V_{solid}^0}{(RT)r}\right) \right. \\ &\quad - c_0 \exp\left(\frac{2\gamma V_{solid}^0}{(RT)r}\right) \left\{ \frac{1}{2(RT)^2} (V_{solid}^0 - V_{solution}^0)^2 \right. \\ &\quad \left. \left. + \frac{1}{2(RT)} \left(\frac{V_{solid}^0}{K} - \beta\right) \right\} \frac{\Delta P_{max}^2}{\mathcal{T}} \int_0^{\mathcal{T}} \frac{2\pi}{\omega} (\sin \omega t)^2 dt \right] = \\ 4\pi r D &\left[ c_{\infty} - c_0 \exp\left(\frac{2\gamma V_{solid}^0}{(RT)r}\right) - c_0 \exp\left(\frac{2\gamma V_{solid}^0}{(RT)r}\right) \frac{\Delta P_{max}^2}{4(RT)} \left\{ \left(\frac{V_{solid}^0}{K} - \beta\right) + \frac{(V_{solid}^0 - V_{solution}^0)^2}{(RT)} \right\} \right] \end{aligned}$$

Note that the above expression is actually correct to ( but not including) terms of  $O(\Delta P_{max}^4)$ , as all dependencies on odd powers of  $\Delta P$  average out to zero for a sinusoidally applied field. More importantly, we observe that even when the bulk concentration in the solution  $c_{\infty}$  is set to  $c_{solid}^0$  corresponding to a concentration where  $r$  is the critical nucleus size, i.e. Eq. 2:

$$\ln \frac{c_{solid}^0}{c_0} = \frac{2\gamma V_{solid}^0}{(RT)r}$$

the average flux will still not vanish if:

$$\left(\frac{V_{solid}^0}{K} - \beta\right) + \frac{(V_{solid}^0 - V_{solution}^0)^2}{(RT)} \neq 0$$

For such an otherwise critical nucleus (where flux will normally be zero), the average flux is calculated to be:

$$\bar{j}_{crit} = \frac{-\pi r \Delta P_{max}^2 D c_0}{(RT)} \exp\left(\frac{2\gamma V_{solid}^0}{(RT)r}\right) \left[ \left(\frac{V_{solid}^0}{K} - \beta\right) + \frac{(V_{solid}^0 - V_{solution}^0)^2}{(RT)} \right]$$

which can be positive if:

$$\left(\frac{V_{solid}^0}{K} - \beta\right) + \frac{(V_{solid}^0 - V_{solution}^0)^2}{(RT)} < 0$$

Eq. 12

And negative otherwise.

For the hexadecane example considered in Povey<sup>2</sup> molar volume in the solid phase is  $292 \times 10^{-6} \text{ m}^3/\text{mole}$  (302 K)<sup>10</sup>. For liquid hexadecane at ambient pressure and at 303 K the molar volume is  $240 \times 10^{-6} \text{ m}^3/\text{mole}$ <sup>11</sup> and  $\beta \cong \frac{(310-295)}{10^8}$  (Figure 6 in Yurtseven and Tilki, 2006<sup>12</sup>). We can't find experimental data for the bulk modulus of solid hexadecane but a plausible value is  $\sim 1.4 \times 10^9 \text{ Pa}$  which gives a value for the inequality Eq. 12 of  $-1.50\text{E-}07 \text{ m}^3 / \text{mol} / \text{Pa}$ , suggesting that the imposition of a harmonically oscillating low pressure field will tend to increase the size of a critical nucleus once it has appeared, thus effectively reducing the value of the critical radius. This effect has

to be balanced against the thermal rectification effects discussed in Povey (2016)<sup>2</sup> where we calculate that heat will flow into a nucleus under the conditions of an oscillating pressure field. An accurate resolution of this problem awaits further experimental investigation.

## XRD investigation of the crystallization of eicosane in 80/20 v/v heptane/toluene

15% v/v of n-eicosane (C<sub>20</sub>, 99% pure) was made up in a 80/20 v/v heptane/toluene (both 99% pure)



Figure 3 Left: Acousto-optic cell situated on the I22 beam line. Middle: Diagram of cell, Right: Off-line corroboration experiment setup - cell dimensions 40 mm dia x 80mm.

Measurements were conducted on the I22 SAXS/WAXS beamline at the Diamond Light Source, Rutherford Appleton Laboratory, Didcot UK using a specially designed acousto-optic cell (Figure 3) The 16-mm diameter, 8-mm thick, 840 material piezo-electric transducers (APC International Ltd, USA) operated off-resonance at 2 MHz . The cover material are borosilicate glass slides which are 1mm thick. Experiments were also performed on anhydrous butter fat, both in the acousto-optic cell described here and in a 1 litre sample, held in a 90 mm id stainless steel pipe insonified magnetically producing a well-defined uniform acoustic field verified using a hydrophone. XRD performed on samples removed from the 1 litre sample agreed with the changes observed in the acousto-optic cell.

### *Acoustic flux calculation*

Maximum flux at 4 W assuming 5% conversion efficiency from electric excitation to acoustic output and a contact diameter with the 16 mm transducer of 1.5 mm, is  $(4 \times 0.05) / (\pi \times (16/1.5)^2 \times 0.0015^2) = 0.25 \text{ kW/m}^2$ . This is around 100 x less than the cavitation threshold for water. Experiments were conducted in larger sample volumes externally to the acousto-optical cell used in the XRD experiments in order to corroborate visually and via speed of sound measurements the effects described below (Figure 3 right).

## Results and Discussion:

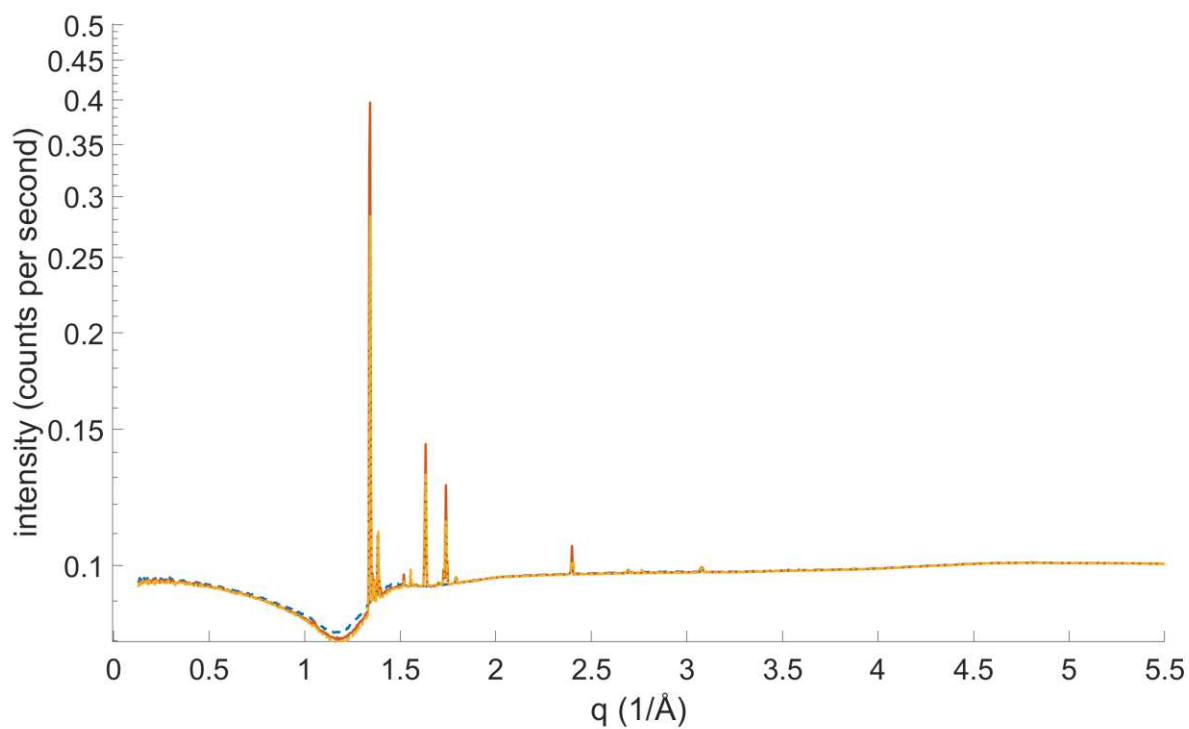


Figure 4 Intensity (background subtracted) plotted against  $q$  for non-sonicated sample (a, dashed line) 8.6 °C non-crystallised sample; (b – continuous line) 5 °C sample crystallised; (c -dot-dash line) 3.8 °C sample crystallised.

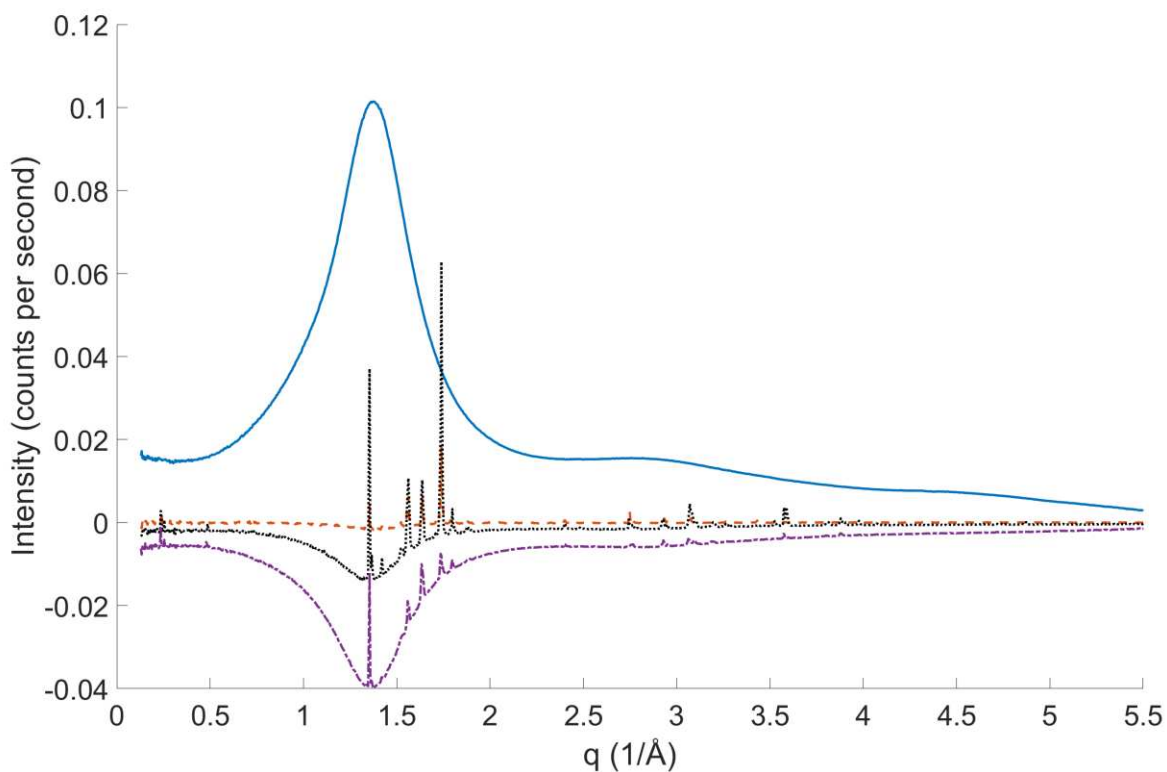


Figure 5 4W insonified sample with Intensity plotted against  $q$  with (a – solid line) 5 °C non-crystallised data; subsequent plots have the data in (a) subtracted; (b – dashed line) 4 °C; (c – dotted line) 1.3 °C and (d – dot-dash line) 0.7 °C.

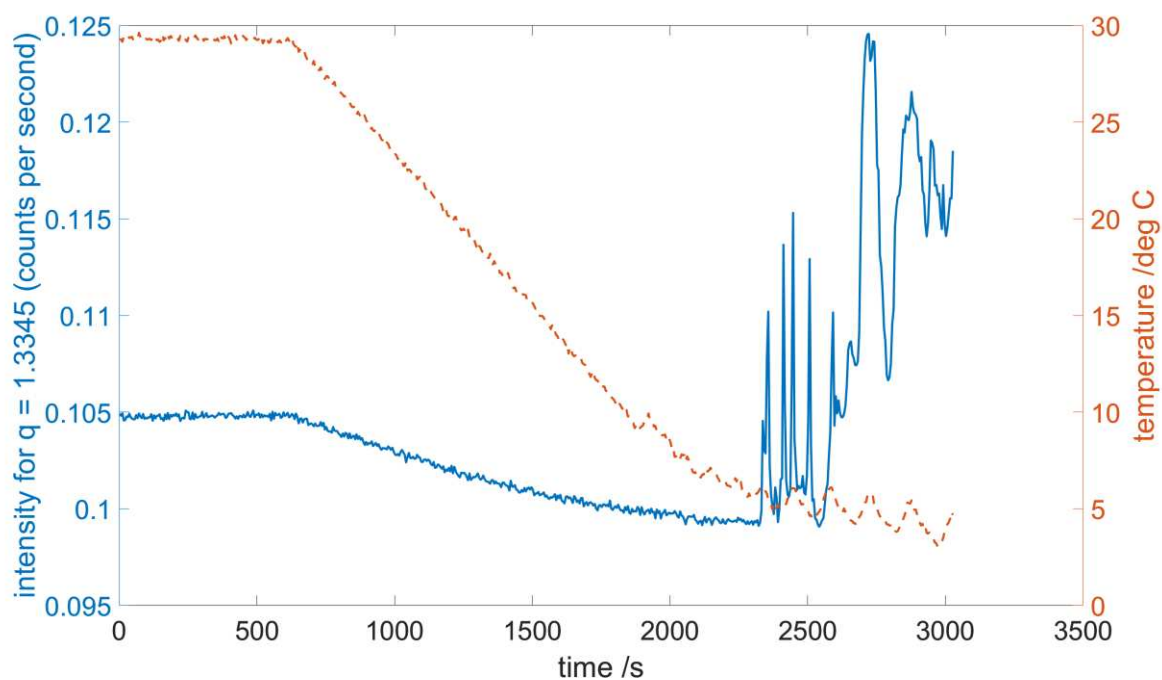


Figure 6 Determination of the temperature at which uncontrolled crystal growth occurs through temperature dependence of the intensity of a single diffraction peak in the unsonicated sample. Red dashed line is temperature and blue solid line is intensity of the signal at  $q = 1.3345$ . In this case the sample crystallised at  $6.05^{\circ}\text{C}$ .

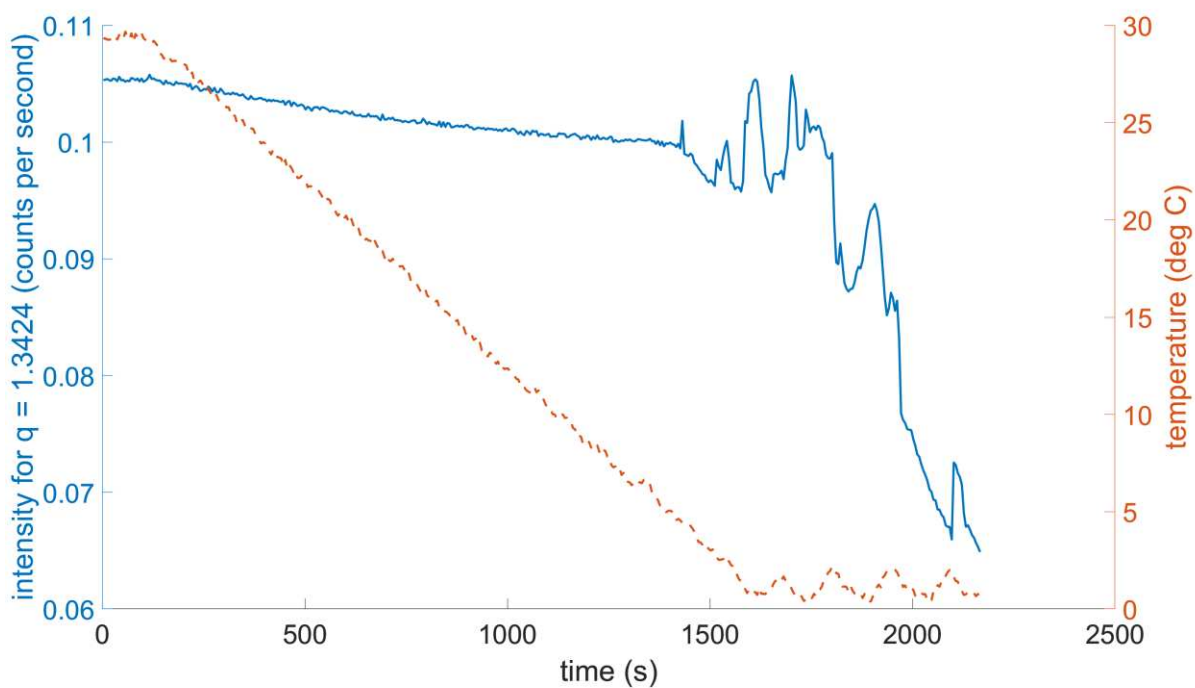


Figure 7 Data for insonified samples  $< 1\text{ W}$  crystallising at  $4.43^{\circ}\text{C}$ ; Red dashed line is temperature and blue solid line is Intensity for  $q = 1.3424$

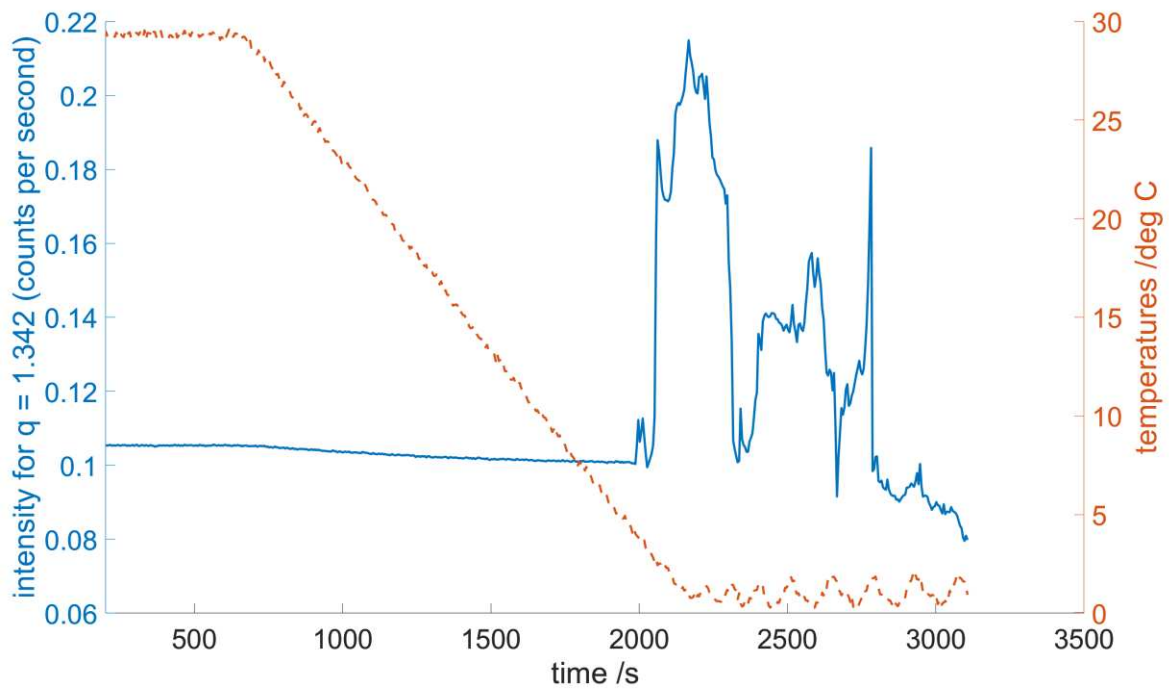


Figure 8 Data for samples insonified @ 4 W crystallising at 4.06 °C. Red dashed line is temperature and blue solid line is Intensity for  $q = 1.3424$

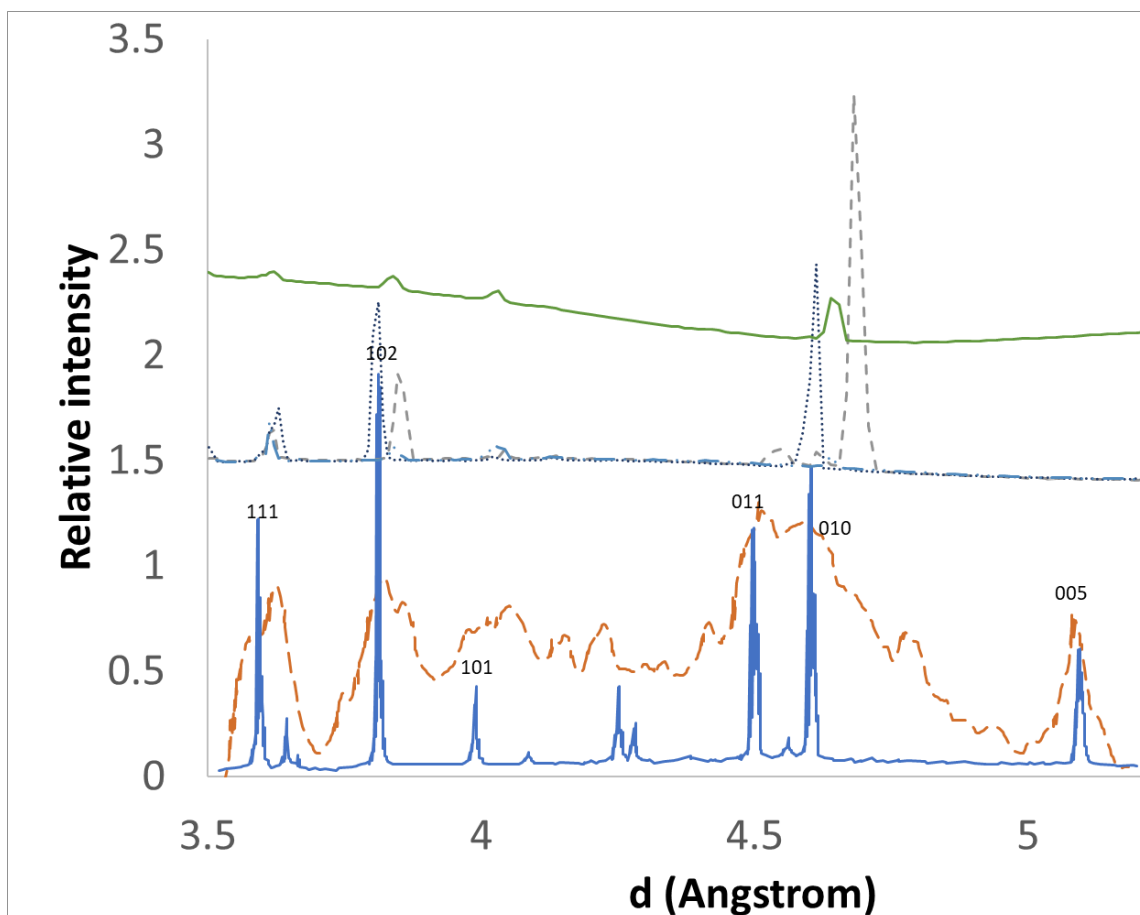


Figure 9 Comparison of Doyle et al data with diffraction pattern obtained in I22 experiments. The intensities of the I22 data are as recorded, with cell and solvent background subtracted. Red large dashed line: Doyle et al (a); blue solid line: Doyle et al (b) Doyle peak assignation associated with Doyle peaks; green small dashes; no ultrasound 4 °C; blue dotted line; <1W ultrasound, 4 °C; blue dash dotted line: 4W ultrasound; green solid line: 4W ultrasound, 0.7 °C.

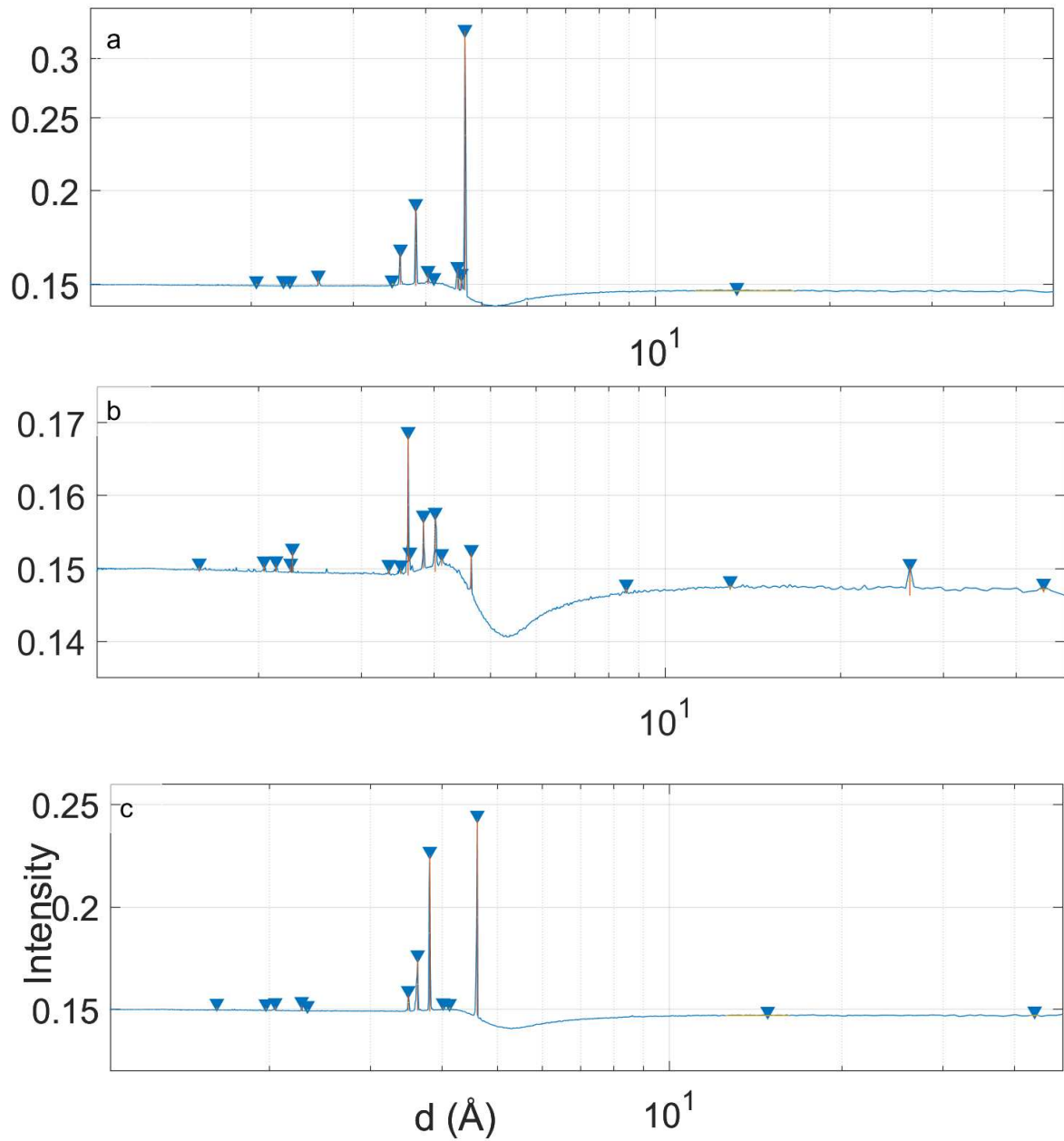


Figure 10 Diffraction pattern, signal intensity, peak position, prominence and width at 4 °C. for (a – top) non-sonicated sample; (b – middle) 4W ultrasound; (c – bottom) <1W ultrasound. Detailed data is provided in Table 2.

Table 1 Peak positions, intensities, widths, prominence, normalised intensity, assigned lattice parameters, calculated dhkl for assigned lattice parameters, and relative to the non-sonicated sample: peak shift and inverse of peak broadening consequent on ultrasonication. These data were obtained using Matlab and plots in Figure 11.

Peak	Tcrystal = 6.05 °C	No ultrasound 4 deg C (run 268)	d (Å)	pk intensity	width (Å)	prominence	Intensity normalised	h	k	l	n	d <sub>hkl</sub> (Å)	Δdhkl (Å)	1/Δw
		0.4549	13.8117	0.1476	5.6451	0.0011	0.4520							
f		3.0780	2.0413	0.1507	0.0095	0.0011	0.4613							
m		2.6931	2.3330	0.1507	0.0116	0.0014	0.4616							
j		1.5191	4.1362	0.1522	0.0146	0.0014	0.4659							
e		2.7638	2.2734	0.1508	0.0052	0.0015	0.4617							
d		1.7939	3.5025	0.1510	0.0311	0.0015	0.4625							
		2.4065	2.6109	0.1533	0.0174	0.0040	0.4694							
g		1.5544	4.0422	0.1555	0.0128	0.0052	0.4762	1	0	1	1	30.45		
		1.3620	4.6133	0.1541	0.0171	0.0063	0.4719							
		1.3816	4.5477	0.1574	0.0388	0.0095	0.4821							
c		1.7350	3.6214	0.1661	0.0197	0.0162	0.5087	1	1	1		26.85		
b		1.6329	3.8478	0.1911	0.0249	0.0418	0.5851	0	1	1	1	24.16		
a		1.3424	4.6807	0.3266	0.0243	0.1793	1.0000	0	1	0	1	4.82		

Ultrasound < 1W 4 deg C (run 267)	Tcrysta l= 4.43 °C													
m		2.6971	2.3296	0.1502	0.0108	0.0008	0.6182						-0.0034	- 1247.5 7
l		0.4235	14.8362	0.1475	3.6454	0.0009	0.6068							
k		0.1447	43.4204	0.1476	1.4542	0.0009	0.6073							
j		1.5230	4.1256	0.1513	0.0276	0.0014	0.6224						-0.0107	77.03
i		3.1879	1.9709	0.1511	0.0079	0.0016	0.6219							
h		3.8829	1.6182	0.1513	0.0038	0.0017	0.6227	1	0	2		57.78		
g		1.5622	4.0219	0.1516	0.0216	0.0018	0.6237	1	0	1		30.45	-0.0203	113.92
f		3.0701	2.0466	0.1517	0.0059	0.0022	0.6241						0.0052	-274.73
e		2.7599	2.2766	0.1522	0.0069	0.0029	0.6264						0.0032	585.52
d		1.7979	3.4948	0.1576	0.0185	0.0083	0.6483						-0.0076	-79.00
c		1.7311	3.6296	0.1750	0.0244	0.0255	0.7200	1	1	1		26.85	-0.0039	212.34
b		1.6486	3.8111	0.2254	0.0190	0.0763	0.9276	0	1	1		24.16	-0.0367	-169.78
a		1.3620	4.6133	0.2430	0.0181	0.0959	1.0000	0	1	0		4.82	-0.0675	-162.85
Ultrasound 4W 4 deg C (Run 269)	Tcrysta l= 4.00 °C													
h		3.9732	1.5814	0.1504	0.0124	0.0008	0.8929	1	0	2		57.78		

k		0.1408	44.6315	0.1476	1.7598	0.0009	0.8765							
		0.4863	12.9196	0.1479	0.2290	0.0009	0.8786							
d		1.7900	3.5102	0.1501	0.0204	0.0009	0.8914					0.0077	-93.21	
e		2.7677	2.2701	0.1504	0.0050	0.0009	0.8929					-0.0032	-5036.18	
		0.7337	8.5636	0.1475	0.0499	0.0009	0.8758							
		1.7272	3.6378	0.1519	0.0060	0.0010	0.9019							
		1.8764	3.3486	0.1502	0.0116	0.0010	0.8918							
f		3.0740	2.0440	0.1507	0.0060	0.0011	0.8947					0.0026	-288.71	
		2.9327	2.1425	0.1507	0.0064	0.0012	0.8948							
j		1.5230	4.1256	0.1517	0.0348	0.0013	0.9007					-0.0107	49.42	
		2.7481	2.2864	0.1524	0.0065	0.0030	0.9050							
		0.2389	26.2953	0.1503	0.5942	0.0040	0.8926							
a		1.3541	4.6400	0.1522	0.0136	0.0051	0.9039	0	1	0		0.0268	-93.28	
b		1.6369	3.8386	0.1569	0.0138	0.0069	0.9320	0	1	1		-0.0092	-89.94	
g		1.5622	4.0219	0.1573	0.0329	0.0078	0.9343					-0.0203	49.74	
c		1.7390	3.6132	0.1684	0.0122	0.0193	1.0000	1	1	1		-0.0082	-132.34	
Lattice parameters according to Doyle et al														
a (Å)		b (Å)	c (Å)	$\alpha$ (°)	$\beta$ (°)	$\gamma$ (°)	V (Å <sup>3</sup> )	$d_{hkl}$	$\lambda$ (Å)					

4.282		4.818	27.412	85.586	68.279	72.607	501							
-------	--	-------	--------	--------	--------	--------	-----	--	--	--	--	--	--	--

Due to problems with the temperature controller, it was not possible to exactly reproduce the temperature-time profile in each run. In addition, the temperature oscillated around isothermal set points, so each run has a separate recording of the temperature, synchronised by timestamps to the diffraction data (Figure 4 to Figure 8 ,).

The straight-forward conclusion from this and other published work is that low power, continuous, non-cavitational ultrasound has a profound effect on nucleation and crystal growth in n-eicosane with a reduction in crystallisation temperature from 6.05 °C in the case of the non-sonicated wax solution; sonicated at less than 1 W, 4.43 °C and sonicated at 4 W 4.00 °C .

However, there is a great deal more to be explained. During the I22 experiments, we found that we could control the appearance and disappearance of crystallites and saw big changes in the electro-mechanical impedance of the transducer associated with the appearance and disappearance of diffraction spots on the 2-D detector. The shifts in the peak positions as detailed Table 1 require further analysis, as do the differences between our data and that of Doyle (Figure 9). The differences are probably because Doyle crystallised their samples from the melt and from dodecane whereas our samples crystallised from heptane/toluene. These solvent effects are interesting in themselves.

Increasing the acoustic power from <1 W to 4 W causes a significant reduction in peak intensity. The application of ultrasound causes the main peak to shift to shorter spacing, less so in the case of the higher applied power.

Due to time limitations and limited access to the I22 SAXS/WAXS beam we were unable to explore these phenomena further and are planning future experiments to examine the impact of insonifying frequency and power in greater detail. We are also planning to model the acoustic field in the sample cell, initial data suggest that the field distribution in the cell is very sensitive to insonifying frequency.

### Small Angle Xray Scattering - SAXS

We have explored the use of dissipative particle dynamics (DPD)<sup>13</sup> in order to simulate the impact of a continuous oscillating pressure field on a box of wax molecules.<sup>14,15,16</sup> Initial results suggest that the oscillating field significantly changes the packing of molecules in the liquid state and that switching off the oscillating field incurs a relatively slow relaxation back to the initial, unsonified state. Such changes in packing, for example from 2L to 3L may be frozen in by cooling the sample, resulting in changes in polymorph and morphology that we have seen in dairy fats. We would expect to see these effects in our SAXS measurements although the results presented below require further explanation.

Our SAXS measurements, carried out simultaneously with the WAXS measurements on the I22 beamline indicate that insonification has a profound effect on the long-range order (Figure 11)

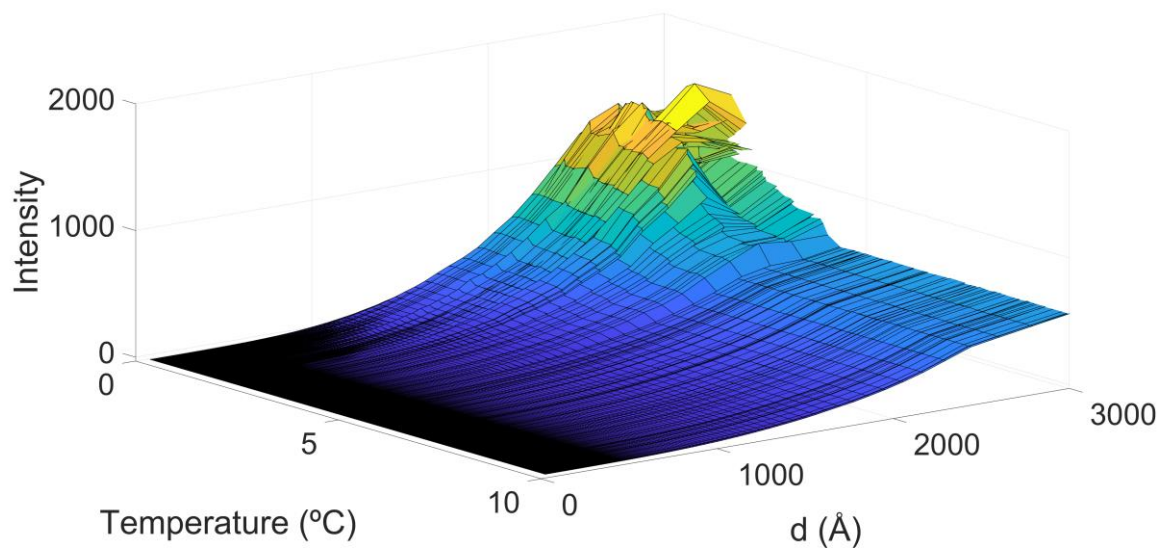
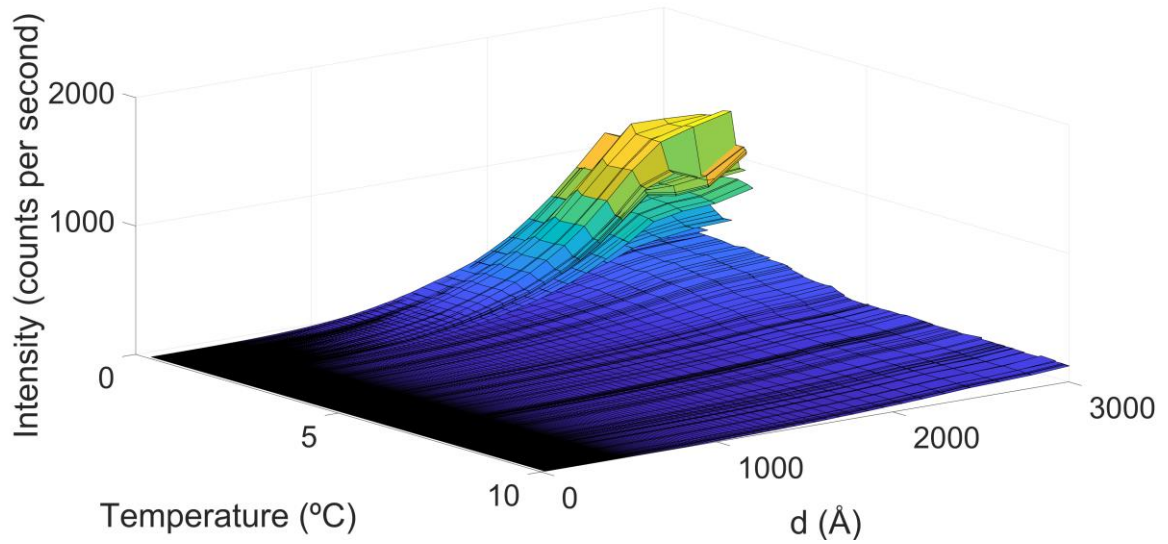
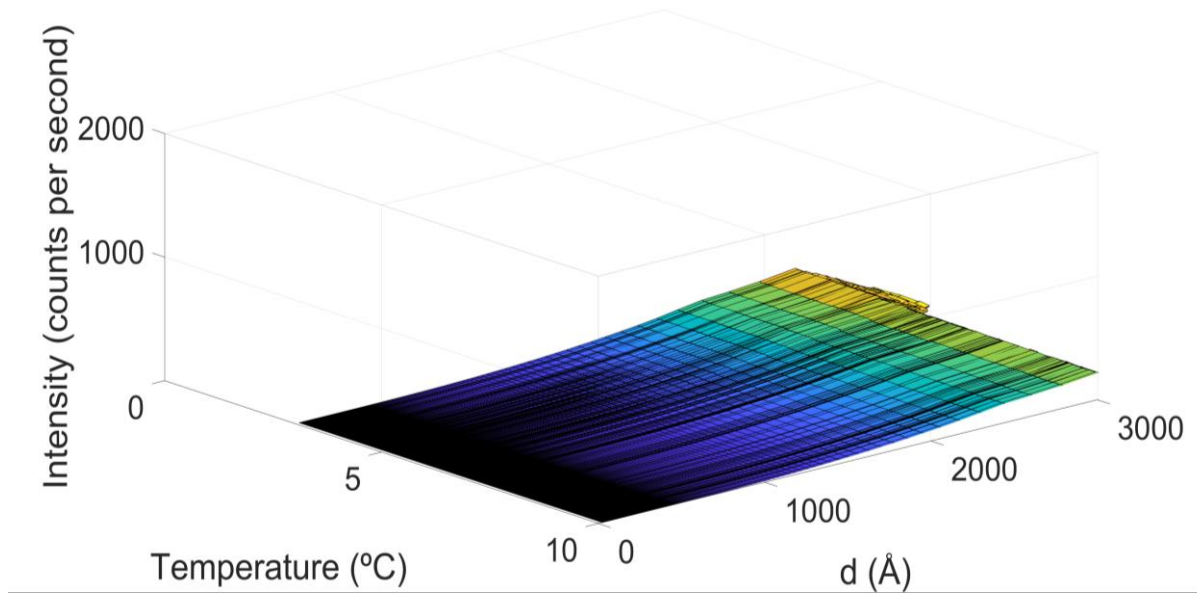


Figure 11 SAXS plots of scattered intensity versus temperature (decreasing) and spacing. From top to bottom (a) no ultrasound; (b) <1W ultrasound and (c) 4W ultrasound.

In the case of very low intensity ultrasound (Figure 11 b), the scattering intensity fluctuates wildly with temperature and the long-range order in the liquid state is very significantly depressed but in the 4W case (Figure 11 c) long range order, even in the melt is significantly increased relative to the unsonicated sample. Once the system has crystallised, the long-range order is significantly increased by the application of ultrasound.

## Conclusions

We show that ultrasound spectroscopy measurements can reveal quantitatively the behaviour of embryos in the 'dead zone' and suggest that measurement time must be fast enough to capture the fleeting presence of the embryos. Whilst the XRD measurement time frame is too long to detect critical behaviour it is evident that low power insonification has dramatic effects on both short range (molecular) and long range (mesoscale) order.

We have outlined an approach which predicts the effect of a harmonically oscillating low power pressure field on critical nucleus size, which ultimately could permit the prediction of the effects of low power, continuous oscillating pressure fields on nucleation and growth in a variety of materials and fields. It is also suggested that DPD<sup>13</sup> offers an approach that accounts for entropy effects and would consequently have greater generality. Unfortunately, we are unable to publish the DPD results for commercial reasons.

Our study of the crystallisation of n-eicosane from solution demonstrates that the application of low power, continuous ultrasound lowers the crystallisation temperature and significantly alters the diffraction pattern. In particular, the influence of solvent on the crystallisation process merits further study. Whilst this study reports only data for n-eicosane, the authors have observed similar phenomena in anhydrous milk fat. We see remarkable effects of ultrasound on mesoscale order, including in the melt in the case of the highest powers used. These phenomena merit further investigation but are consistent with DPD results.

Combining ultrasound pitch and catch speed of sound measurements with low power harmonically oscillating pressure fields to monitor and control nucleation presents the prospect of entirely new industrially significant methods of process control in crystallisation. It also offers new insights into nucleation processes in general. However, for the acoustic control technique to be applied widely, further theoretical and modelling work will be necessary since at present, we are unable to predict the precise effect of low power ultrasound in any given situation.

## Acknowledgements

We are grateful to Dr Nick Terrill and Dr Tim Snow (Diamond Light Source) for assistance and advice (Diamond I22 sm27656-2 Tuning crystal nucleation) and to Arla Foods (Dr Ulf Andersen) for support for a postdoctoral position. We are grateful to Lewtas Science & Technology Ltd for funding preliminary DPD work at Hartree.

## Bibliography

<sup>1</sup> M. Povey and K. Lewtas, US 2022/0143528 A1 (2022).

<sup>2</sup> M.J.W. Povey, J. Chem. Phys. **145**, (2016).

<sup>3</sup> M.J.W. Povey, Curr. Opin. Colloid Interface Sci. **28**, 1 (2017).

<sup>4</sup> S.R. Haqshenas, I.J. Ford, and N. Saffari, J. Chem. Phys. **145**, 024315 (2016).

- <sup>5</sup> S.R. Haqshenas, I.J. Ford, and N. Saffari, *J. Chem. Phys.* **148**, 024102 (2018).
- <sup>6</sup> T.L. Threlfall and S.J. Coles, *CrystEngComm* **18**, 369 (2016).
- <sup>7</sup> M.L. Parada, A. Sadeghpour, J. Vieira, and M. Povey, *J. Phys. Chem.* **Submitted**, (2018).
- <sup>8</sup> T.L. Threlfall and S.J. Coles, *CrystEngComm* **18**, 369 (2016).
- <sup>9</sup> F. Sheng, *Ultrason. Spectrosc. Situ Part. Sizing Cryst. Process Monit.* (2012).
- <sup>10</sup> H. Yurtseven and O. Tilki, *High Temp. Mater. Process.* **26**, 123 (2007).
- <sup>11</sup> G.P. Dubey and M. Sharma, *Int. J. Thermophys.* **29**, 1361 (2008).
- <sup>12</sup> H. Yurtseven and Ö. Tilki, *High Temp. Mater. Process.* **26**, 123 (2007).
- <sup>13</sup> R.D. Groot and P.B. Warren, *J. Chem. Phys.* **107**, 4423 (1997).
- <sup>14</sup> M.A. Seaton, I. Halliday, and A.J. Masters, *J. Phys. A Math. Theor.* **44**, (2011).
- <sup>15</sup> D.J. Bray, R.L. Anderson, P.B. Warren, and K. Lewtas, *J. Chem. Theory Comput.* **16**, 7109 (2020).
- <sup>16</sup> D.J. Bray, R.L. Anderson, P.B. Warren, and K. Lewtas, *J. Phys. Chem. B* **126**, 5351 (2022).

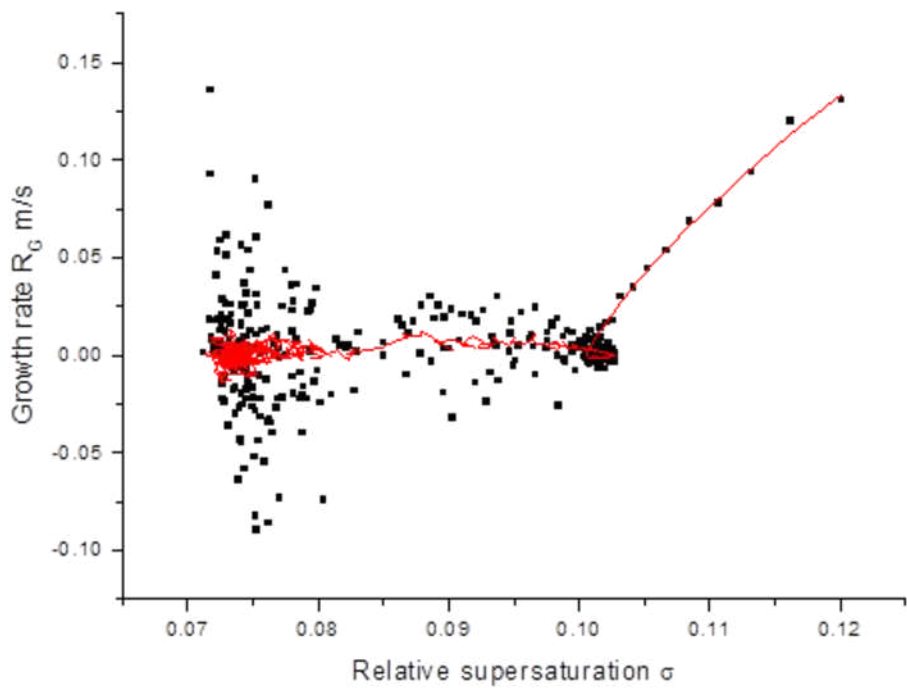
## Data Availability Statement

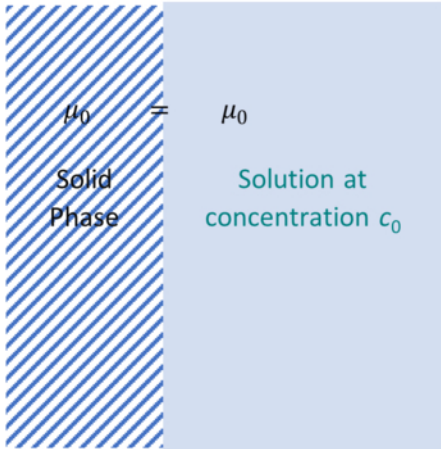
The data that supports the findings of this study are available within the article and its supplementary material

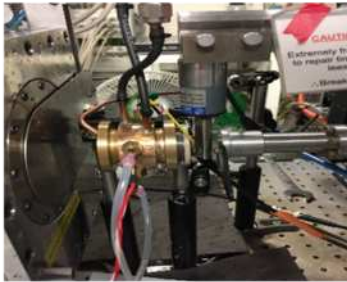
## Supplementary material

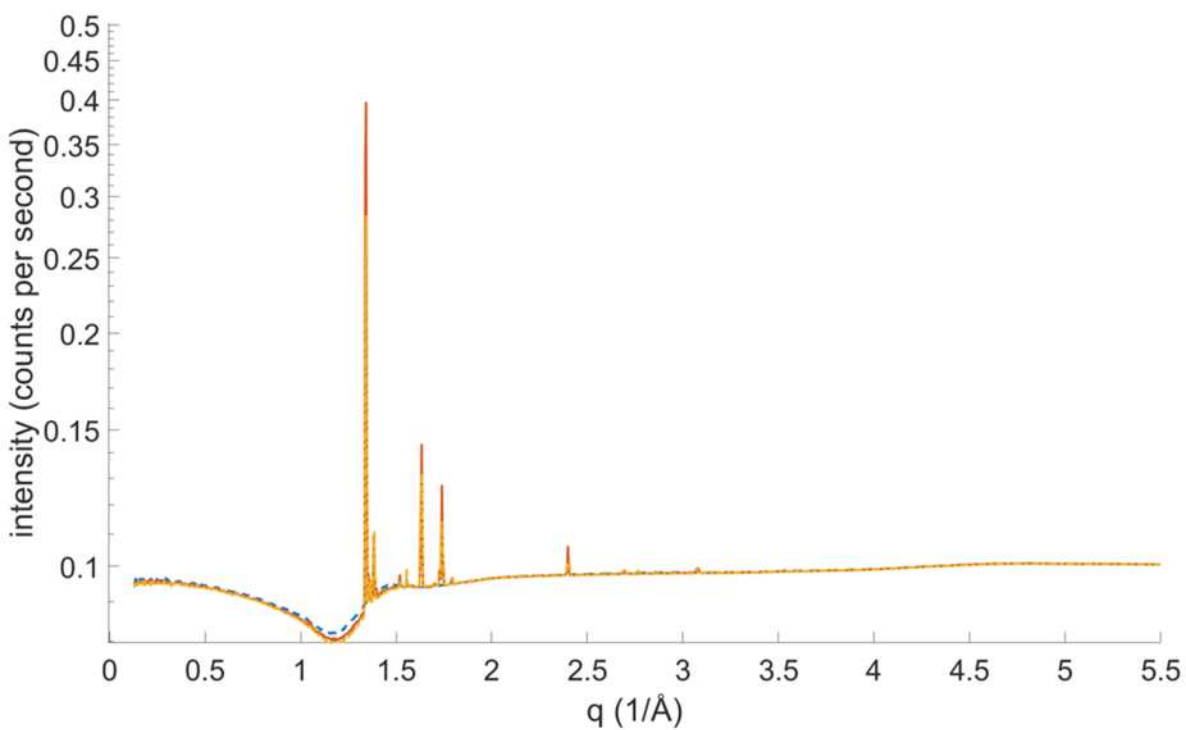
The full XRD data set and analyses can be accessed here [https://leeds365-my.sharepoint.com/:f/g/personal/prc6mp\\_leeds\\_ac\\_uk/Euo9JNyoA3pCh9RK-ObevswBgcolIXWTN83\\_gcdeOwtMHg?e=gsPav3](https://leeds365-my.sharepoint.com/:f/g/personal/prc6mp_leeds_ac_uk/Euo9JNyoA3pCh9RK-ObevswBgcolIXWTN83_gcdeOwtMHg?e=gsPav3) .

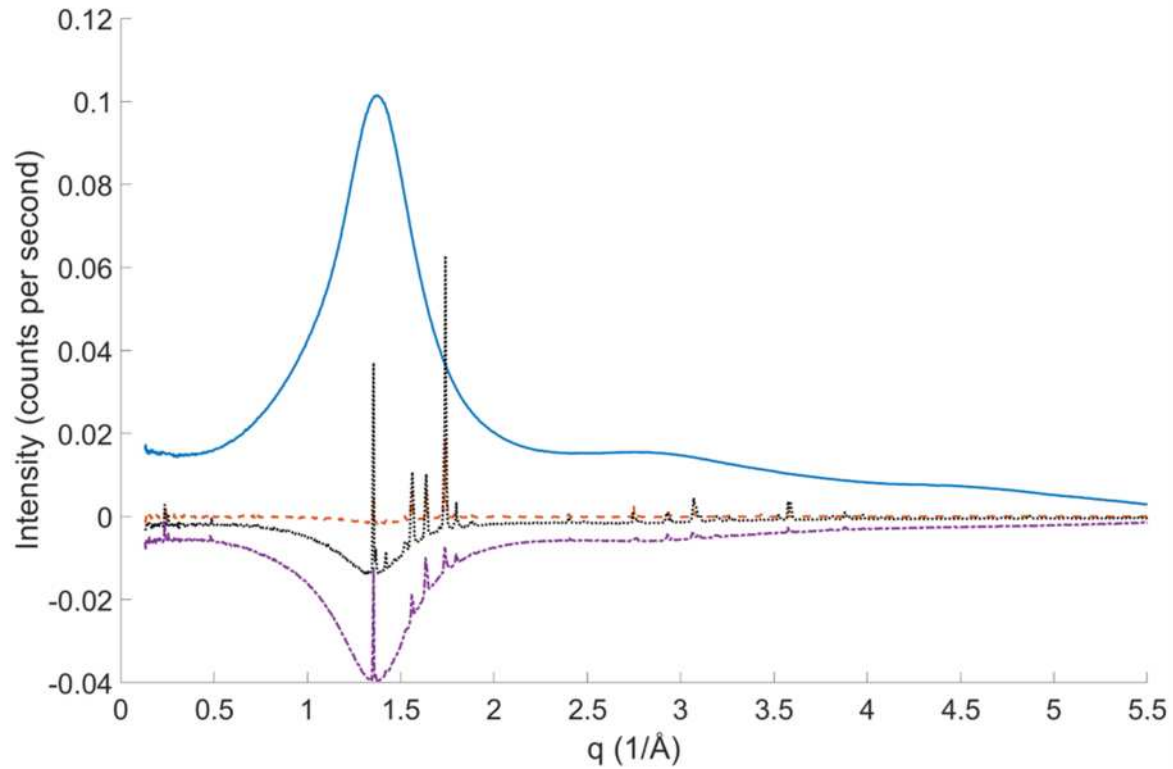
The full data set for the copper sulphate pentahydrate study is available in Fei Sheng's thesis paper copy from the British Library.<sup>9</sup>

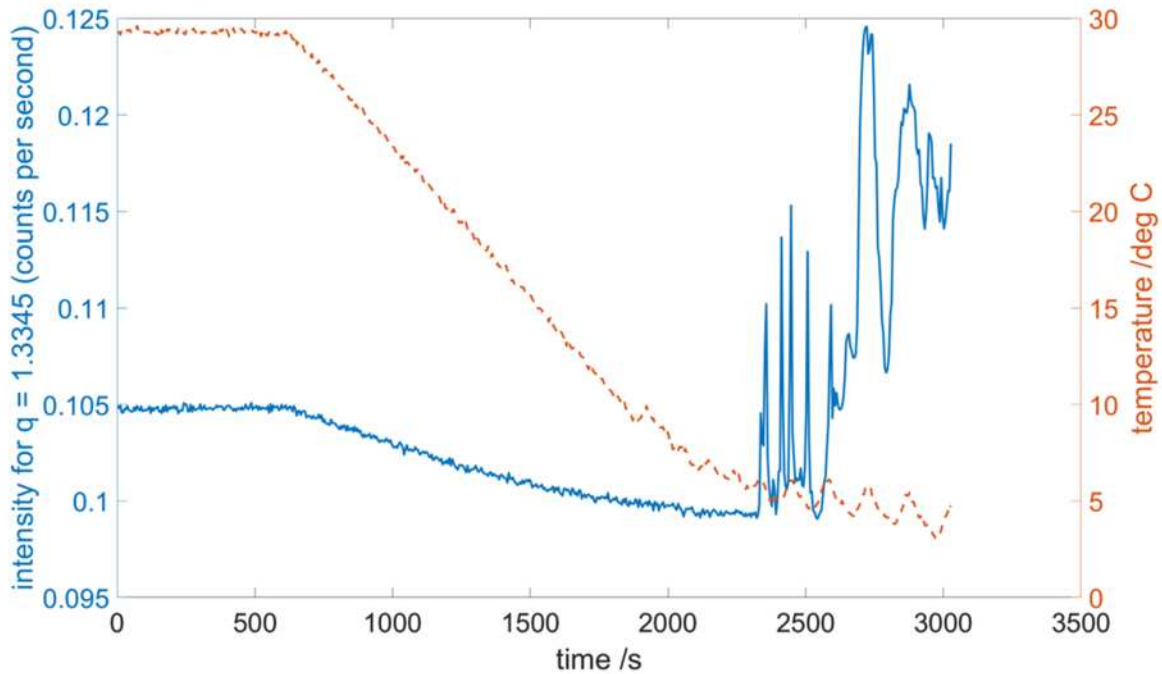


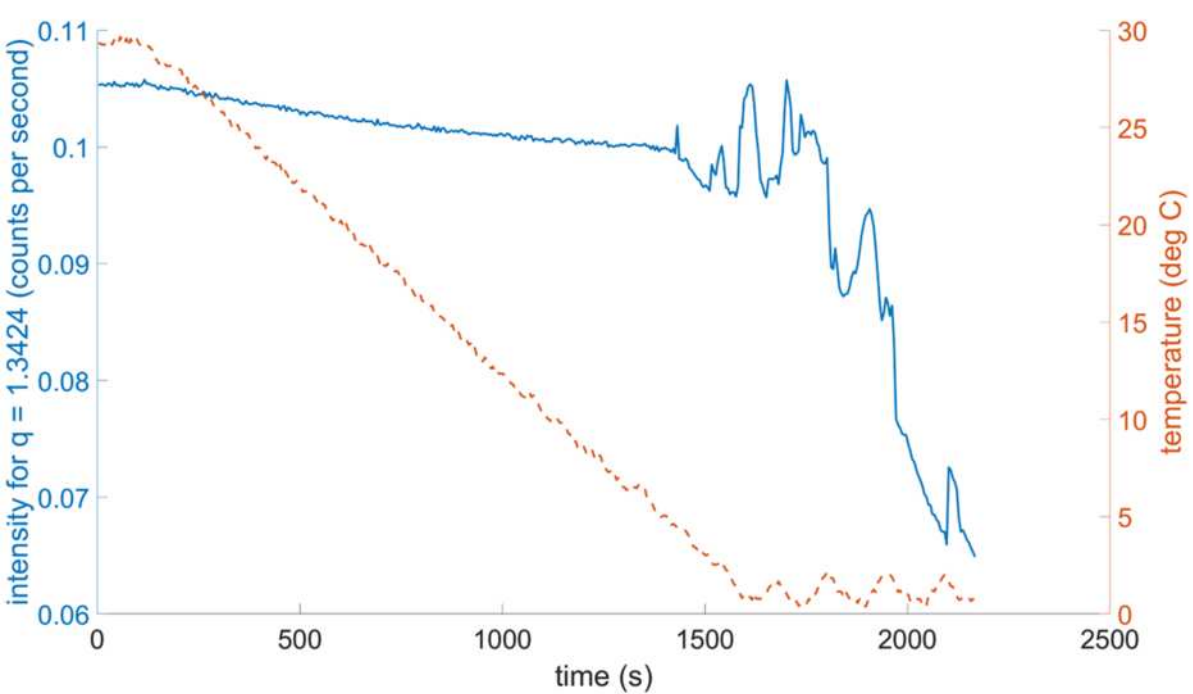


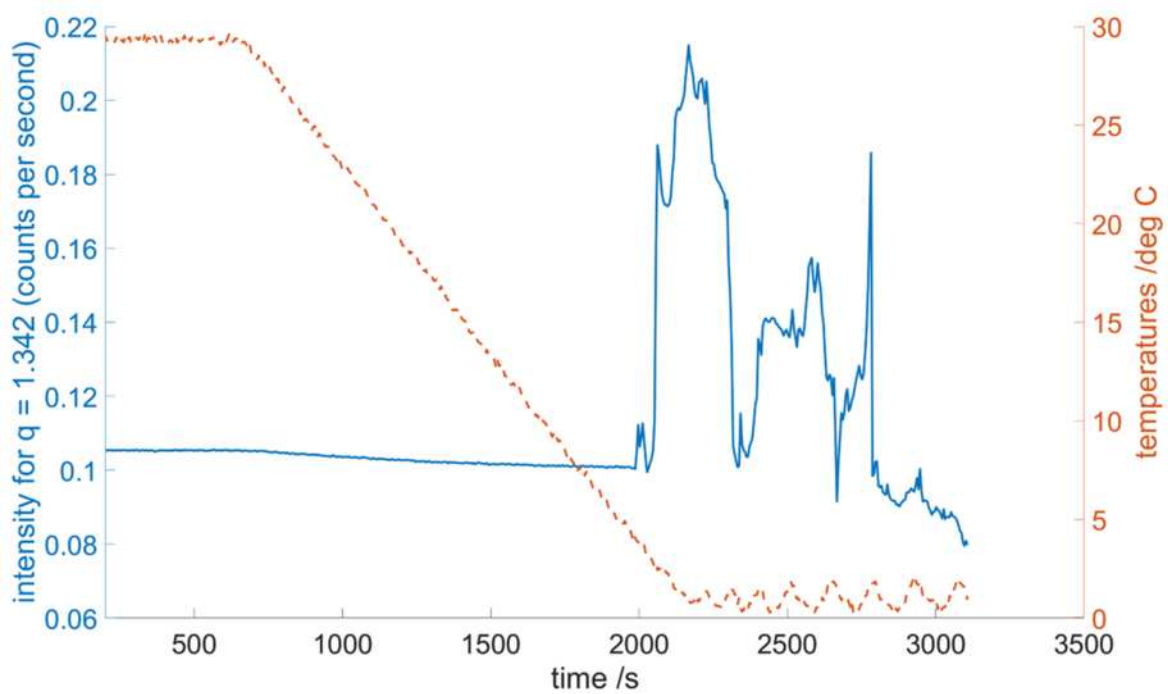


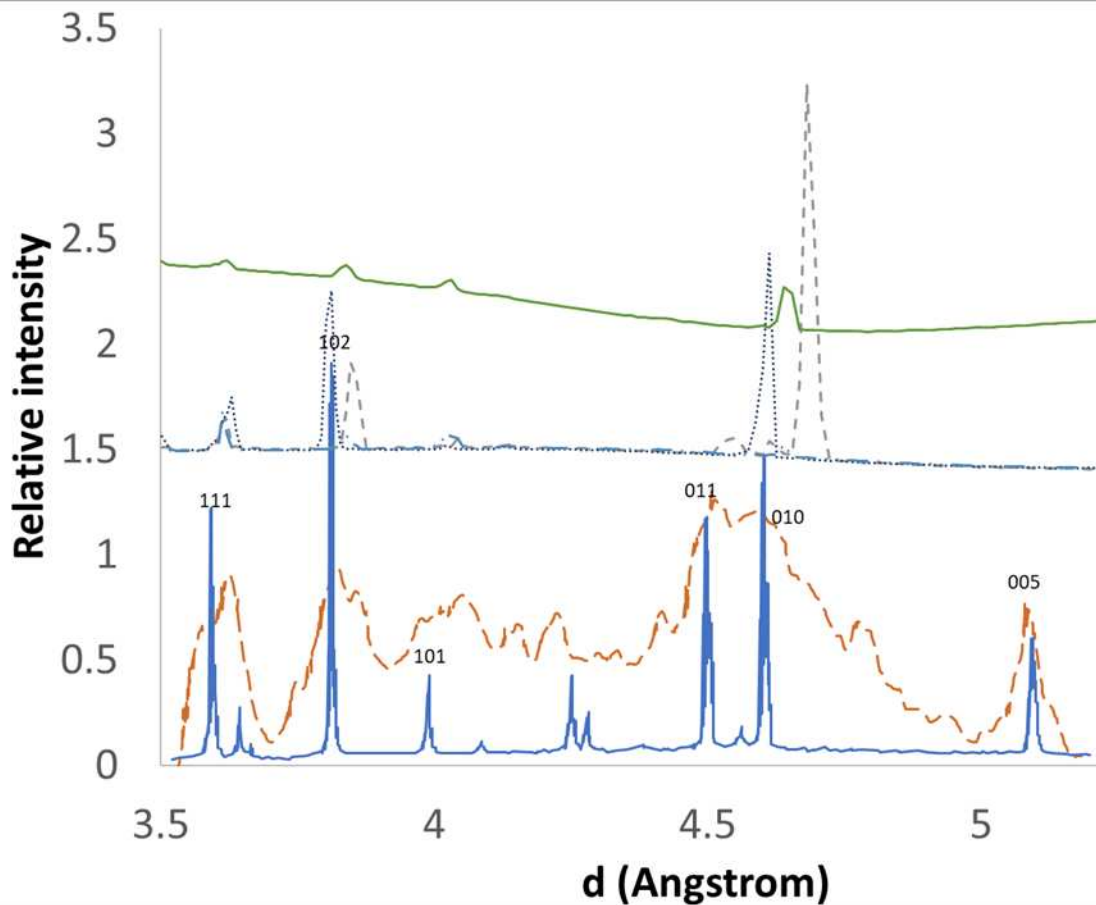


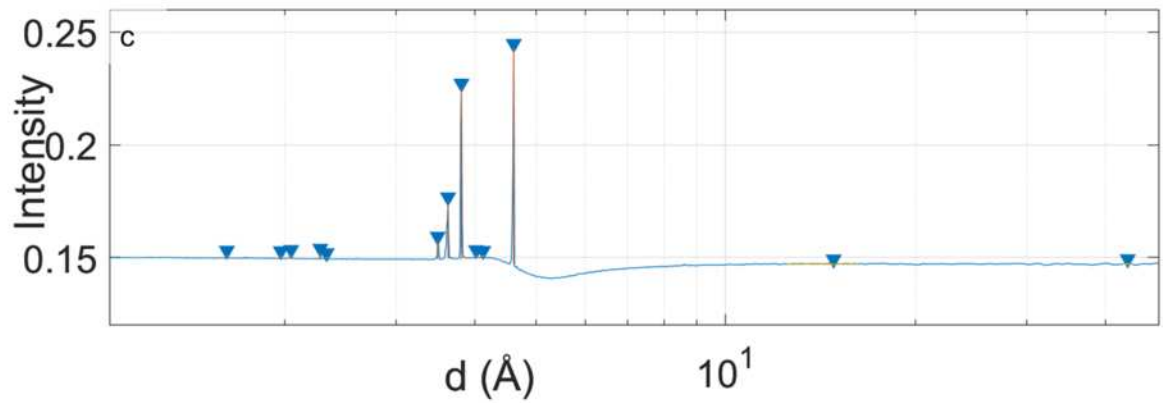
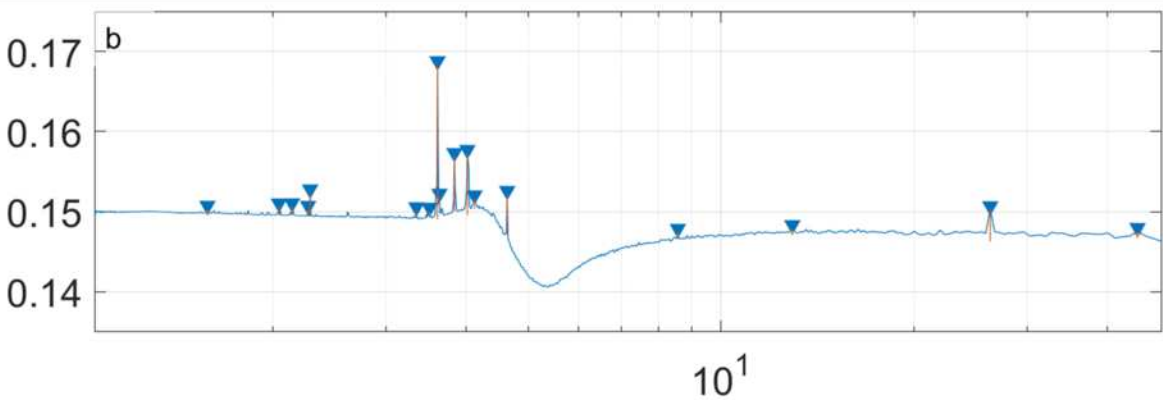
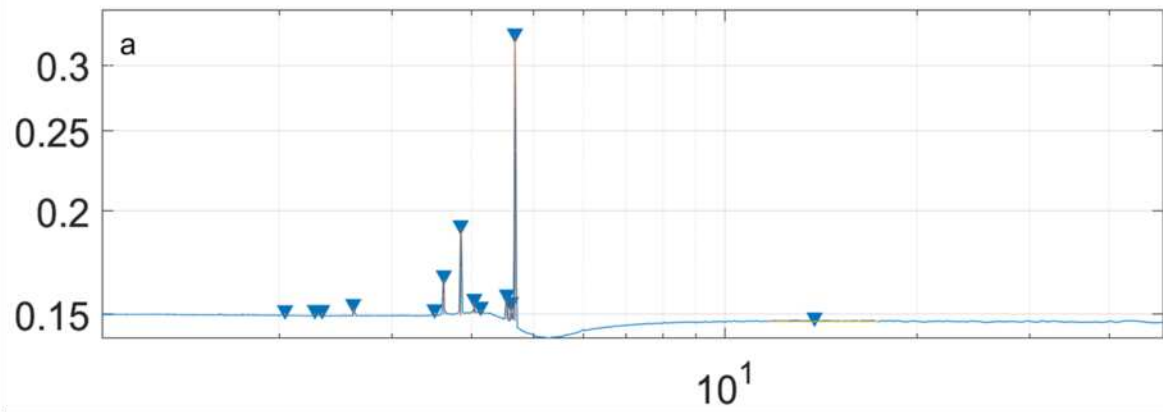




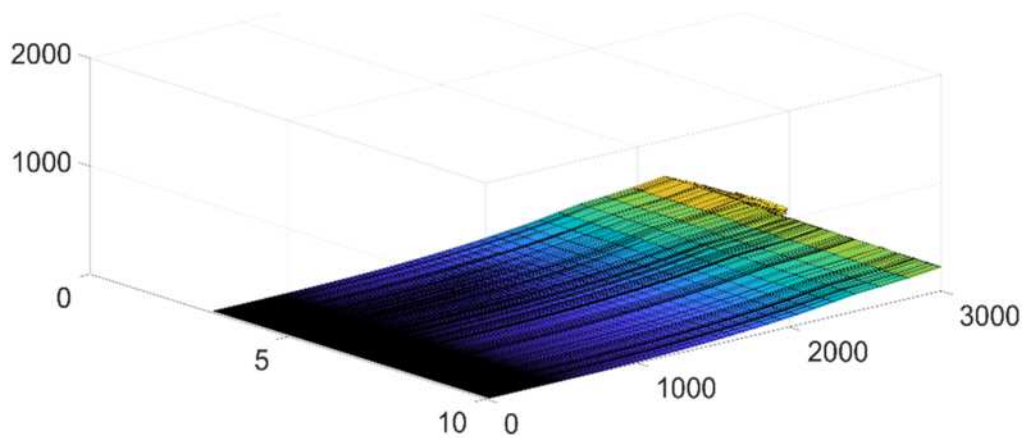




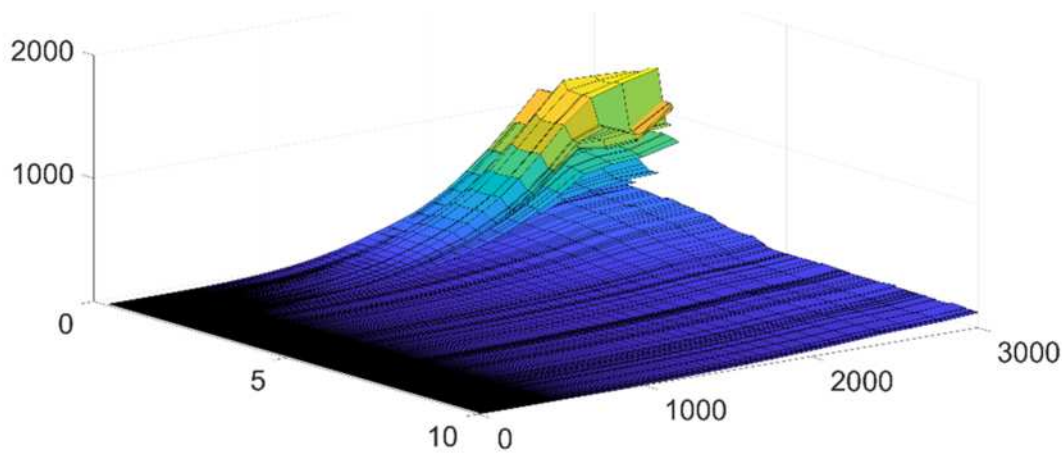




A



B



C

